Human Receptor-Interacting Serine/Threonine-Protein Kinase 2 (RIPK2)

A Target Enabling Package (TEP)

Gene ID / UniProt ID / EC	8767 / O43353 / -
Target Nominator	SGC Internal Nomination
SGC Authors	Peter Canning, Daniel M. Pinkas, Joshua C. Bufton, Sarah Picaud, Jennifer A. Ward, Catherine Rogers, Benedict-Tilman Berger, Stefan Knapp, Susanne Muller-Knapp, Paul E. Brennan, Kilian V. M. Huber, Panagis Filippakopoulos, Alex N. Bullock
Collaborating Authors	Matous Hrdinka[1], Qui Ruan[2], Chalada Suebsuwong[3], Lisa Schlicher[1], Bing Dai[2], Jenny L. Maki[2], Soumya S. Ray[4], Danish Saleh[5], Sameer Nikhar[6], Tobias Schwerd[7], Holm H.Uhlig[7], Gregory D. Cuny[6], Alexei Degterev[2], Mads Gyrd-Hansen[1]
Target PI	Alex N. Bullock (SGC Oxford)
Therapeutic Area(s)	Inflammatory diseases
Disease Relevance	Mutations in the NOD2-RIPK2 pathway identify RIPK2 a potential therapeutic target in auto-immune and inflammatory conditions such as Crohn's disease, Blau syndrome, early-onset osteoarthritis and multiple sclerosis.
Date Approved by TEP Evaluation Group	13th June 2018
Document version	Version 3
Document version date	October 2020
Citation	Peter Canning, Daniel M. Pinkas, Joshua C. Bufton, Sarah Picaud, Jennifer A. Ward, Catherine Rogers, … Alex N. Bullock. (2018). Human Receptor-Interacting Serine/Threonine-Protein Kinase 2 (RIPK2); A Target Enabling Package. Zenodo. http://doi.org/10.5281/zenodo.1344501
Affiliations	1. Ludwig Institute for Cancer Research, Nuffield Department of Clinical Medicine, University of Oxford 2. Department of Developmental, Molecular & Chemical Biology, Tufts University School of Medicine 3. Department of Chemistry, Science and Research Building 2, University of Houston 4. Center for Neurologic Diseases, Department of Neurology, Brigham & Women's Hospital and Harvard Medical School 5. Medical Scientist Training Program and Program in Neuroscience, Sackler School of Graduate Biomedical Sciences, Tufts University School of Medicine 6. Department of Pharmacological and Pharmaceutical Sciences, Science and Research Building 2, University of Houston 7. Translational Gastroenterology Unit, Nuffield Department of Medicine and Department of Pediatrics, John Radcliffe Hospital, University of Oxford

USEFUL LINKS

(Please note that the inclusion of links to external sites should not be taken as an endorsement of that site by the SGC in any way)

For more information regarding any aspect of TEPs and the TEP programme, please contact teps@thesgc.org

SUMMARY OF PROJECT

RIPK2 inflammatory signalling downstream from the bacteria-sensing receptors NOD1 and NOD2 is associated with auto-immune and inflammatory conditions. RIPK2 inhibition has shown promise in disease models of inflammatory bowel disease and multiple sclerosis. In this TEP, we reveal a lack of correlation between inhibitor efficacy in cells and their potency using in vitro kinase assays. We show that RIPK2 kinase activity is in fact dispensable for NOD2 inflammatory signalling and that RIPK2 inhibitors function instead by antagonizing XIAP-binding and ubiquitination of RIPK2. We characterise the molecular basis for this effect. We also solved the first crystal structure of the RIPK2 kinase domain and applied a range of biochemical and cellular assays to profile type I and type II RIPK2 kinase inhibitors. Overall, our study illustrates how to target the ATP-binding pocket in RIPK2 to interfere with the RIPK2-XIAP interaction for modulation of NOD signalling.

SCIENTIFIC BACKGROUND

Signalling Pathway

The intracellular bacteria-sensing receptors NOD1 and NOD2 stimulate pro-inflammatory signalling through the RIPK2 kinase in response to binding bacterial peptidoglycans (1). The activation of RIPK2 is mediated through K63-linked ubiquitination by the E3 ligase XIAP, which facilitates additional linear (Met1-linked) ubiquitination by LUBAC (2). These modifications enable the RIPK2 complex to recruit kinases TAK1 and IKK for downstream activation of MAPK and NF-κB pathways, respectively (**Fig. 1**).

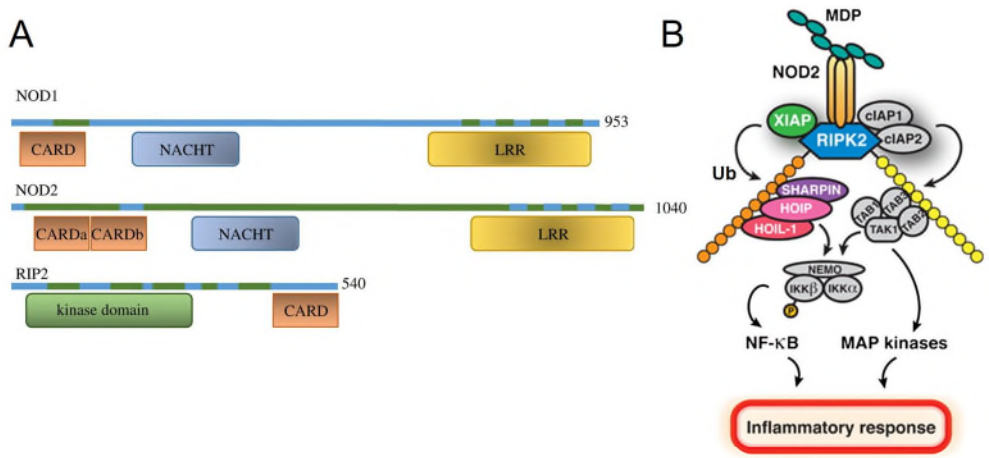

Fig. 1. NOD-RIPK2 signalling domains. (**A**) domain organisation of NOD1/2 and RIPK2. (**B**) Schematic for NOD2-RIPK2 signalling.

Genetic linkage

Genetic variants in NOD2 are the strongest susceptibility factors to Crohn's disease (3,4). While many variants appear loss of function, activating NOD2 mutations are found in pediatric Crohn's disease (5) as well as the monogenic auto-inflammatory disease Blau syndrome, characterized by early-onset granulomatous arthritis, uveitis, and dermatitis (6). A hyperactivating RIPK2 N104D substitution is also associated with early-onset osteoarthritis (7). Amplification of RIPK2 on chromosome 8 is found in 38% of breast cancers and is associated with poor prognosis (8). Knockdown of RIPK2 in these breast cancer cells supported its oncogenic function (8).

TEP Rationale

Recent data from our group and others demonstrated that XIAP-mediated RIPK2 ubiquitination and downstream signalling could be blocked by small molecule kinase inhibitors suggesting a critical role for the catalytic activity of RIPK2 (9-11). Moreover, such inhibitors showed benefits in mouse models of multiple sclerosis (10) and Crohn's Disease-like ileitis (11) increasing interest in RIPK2 as a new therapeutic target. However, our studies also revealed a lack of correlation between inhibitor potency in in vitro kinase assays and inhibitor efficacy in cellular reporter assays creating uncertainty for further structure-activity

relationship (SAR) studies (9). Here, we address this issue by demonstrating that RIPK2 kinase activity is dispensable for NOD2 inflammatory signalling and that efficacious RIPK2 inhibitors function instead by antagonizing XIAP-binding for RIPK2 ubiquitination. We establish a model for the RIPK2-XIAP interaction and directions for small molecule RIPK2 inhibitor development.

RESULTS – THE TEP

Proteins purified

RIPK2 kinase domain (used for crystallography and assays)
Human RIPK2 (residues 3–317 or residues 8-317) was cloned into pFB-LIC-Bse and prepared by baculoviral expression. RIPK2 protein was purified sequentially by nickel affinity and size-exclusion chromatography. The kinase domain displayed heterogeneous phosphorylation at up to 5 sites which could be dephosphorylated by lambda phosphatase. Note, DNA sequencing of the RIPK2 construct spanning residues 3-317 revealed the expected wild-type sequence, whereas the shorter construct spanning residues 8-317 was found to have a mutation R171C in the kinase activation loop.

XIAP BIR2 domain (used for assays)
Human XIAP BIR2 domain (residues 124-242) was cloned into the pGTVL2 vector in frame with N-terminal 6xHIS and GST tags. Protein was expressed in E. coli (BL21DE3) cells and purified either by batch binding to glutathione sepharose or by sequential nickel affinity and size-exclusion chromatography.

XIAP BIR2 D214S mutant domain (used for assays)
The D214S mutant was prepared similarly to the wild-type XIAP BIR2 domain.

Structural data

1. Dephosphorylated RIPK2 kinase domain a.a. 8-317 bound to ponatinib (4C8B, 2.75 Å)
2. Phosphorylated RIPK2 kinase domain a.a. 3-317 bound to CSR35 (6ES0, 2.38 Å)
3. Phosphorylated RIPK2 kinase domain a.a. 3-317 bound to CLSP18 (6FU5, 3.26 Å)

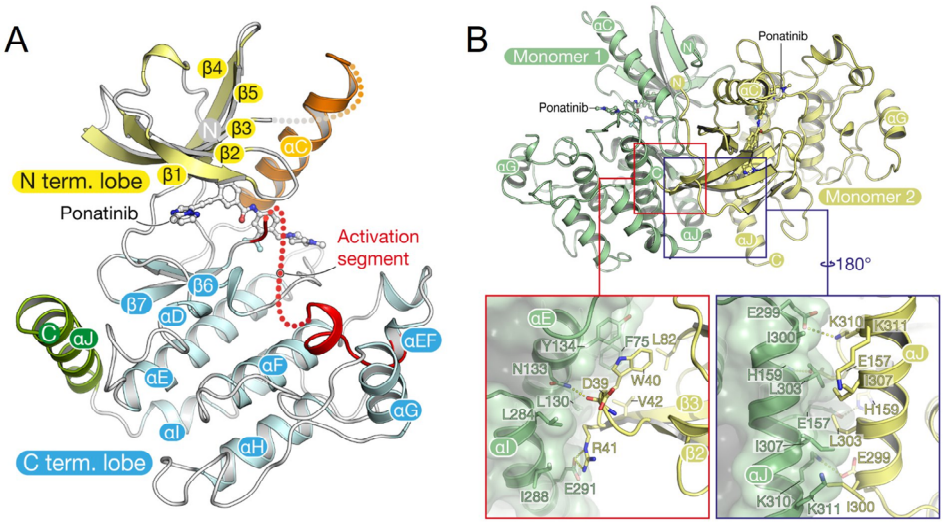

Fig. 2. Dimeric structure of RIPK2. (**A**) Structural features of the RIPK2 kinase domain. (**B**) Dimeric packing of the RIPK2 kinase domain.

The RIPK2-ponatinib complex was the first structure solved for this kinase. RIPK2 exhibits the canonical bilobal kinase fold followed by a 16-residue αJ helix that packs alongside the loop connecting the αD and αE helices (**Fig. 2**). Interestingly, RIPK2 contains several unusual sequence changes in its catalytic motifs that are not conserved in other RIPKs. The typical HRD triad in the catalytic loop is changed to HHD, while the

activation loop APE motif is changed to PPE. The RIPK2 structure reveals a homodimeric packing arrangement consistent with the dimeric state observed in solution by analytical gel filtration (**Fig. 3**). The protein interface is highly symmetrical with the two active sites facing in opposite directions and rotated approximately 90° relative to one another. Binding is supported by the αJ helices, which pack against each other in an antiparallel fashion, and form both hydrophobic and hydrogen bonding interactions.

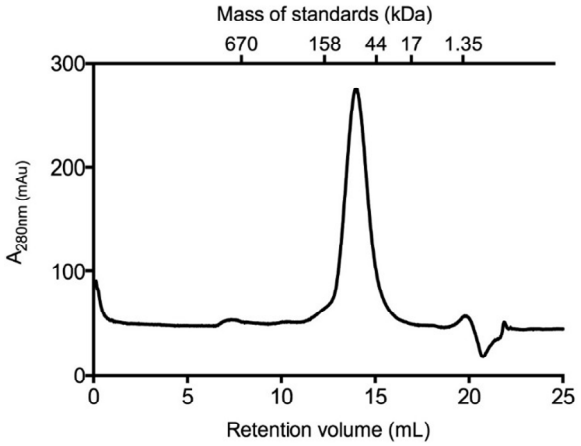

Fig. 3. RIPK2 is dimeric in solution. Analytical gel filtration trace of RIPK2 using a superdex 200 10/300 GL column. The retention volume of RIPK2 was compared to MW standards.

RIPK2 structures with type II inhibitors ponatinib and CSR35 showed a "DFG-Asp out, αC-Glu in" conformation, whereas type I inhibitor CSLP18 was bound to a "DFG-Asp in, αC-Glu in" conformation. Electron density for much of the activation loop was missing in all structures irrespective of whether the protein used for crystallisation was dephosphorylated with lambda phosphatase (ponatinib complex) or left with heterogeneous phosphorylation (CSR35 and CSLP18 complexes). Structural details of the inhibitor binding modes are provided under chemical matter.

Assays of inhibitor potency

Thermal shift assay

A fluorescence-based thermal shift assay (differential scanning fluorimetry (DSF)) was performed as an initial screen to identify potential RIPK2 inhibitors. In this assay, the previously reported RIPK2 inhibitor gefitinib yielded a thermal shift (ΔT_m) value of 9.5°C. However, we found the most potent inhibitor was ponatinib with a ΔT_m value of 23.1°C.

ADP-Glo in vitro kinase assays

An ADP-Glo (Promega) in vitro kinase assay was performed to determine inhibitor IC_{50} values. In this assay, the ADP produced from the kinase reaction is converted to a luminescent signal (**Fig. 4A-B**).

NOD2-HEK-Blue activation assay

To monitor RIPK2 inhibition in cells, we measured the downstream activation of NFκB in HEKBlue cells, which expressed NOD2 and a NFκB-SEAP reporter. In this assay, secreted embryonic alkaline phosphatase (SEAP) is used as a reporter of gene expression which acts on QUIATI-Blue detection media to produce a blue/purple colour detectable using a spectrophotometer (**Fig. 4C**).

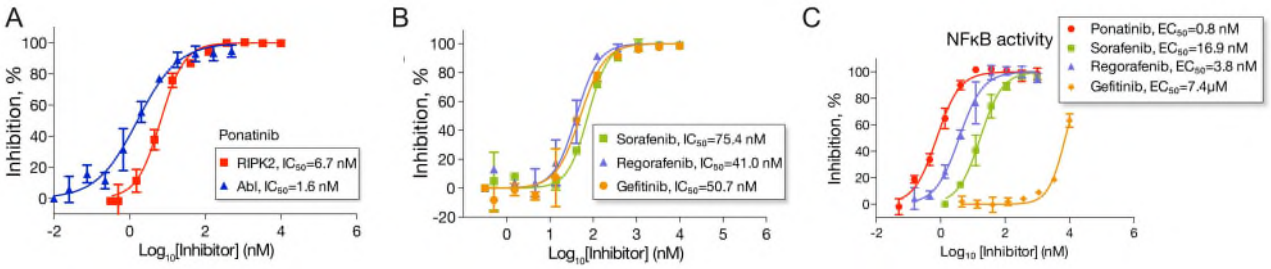

Fig. 4. Comparison of enzymatic and cellular assays for RIPK2. (**A**) ADP-Glo in vitro kinase assay testing ponatinib inhibition of Abl and RIPK2 kinases. (**B**) ADP-Glo assay for RIPK2 inhibition by other clinically-used kinase inhibitors. (**C**) NOD2-HEK-Blue activation assay testing selected inhibitors in HEK293 cells. Gefitinib activity is notably less potent against RIPK2 in cells compared to the in vitro ADP-Glo assay.

Comparison of the in vitro kinase assay and cellular reporter assay revealed remarkable differences (**Fig. 4**). In the kinase assay, the IC_{50} value of gefitinib (50.7 nM) was between those of regorafenib (41.0 nM) and sorafenib (75.4 nM). By contrast the cellular EC_{50} value for gefitinib (7.4 µM) was significantly weaker than those of regorafenib (3.8 nM) and sorafenib (16.9 nM). All of these compounds are FDA approved drugs and therefore have been optimised for cellular and in vivo activity. A striking lack of correlation between in vitro kinase and cellular data for RIPK2 inhibitors was also observed for a set of structurally similar CSLP analogs (**Fig. 5**).

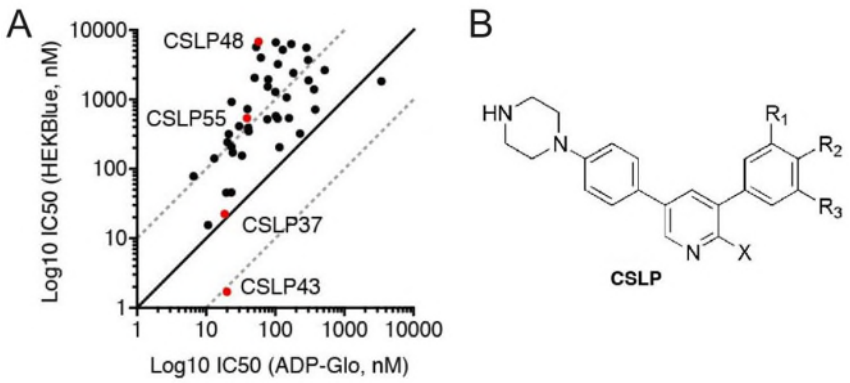

Fig. 5. Lack of correlation for inhibitor potencies measured using the ADP-Glo and cellular HEKBlue reporter assays. (**A**) Correlation plot for different CSLP series compounds. Selected compounds illustrating lack of correlation are highlighted red and labelled. (**B**) General scaffold for the CSLP inhibitor series.

RIPK2 nanoBRET target engagement assay

A nanobret (nano-bioluminescence resonance energy transfer) target engagement assay for RIPK2 was developed through SGC collaboration with Matt Robers at Promega (12). In this assay, cells were transfected with a RIPK2 transgene fused to NanoLuc luciferase and a BRET signal induced by addition of a cell-permeable fluorescent tracer compound SGC-590001 derived from ponatinib (**Fig. 6**). The binding potencies of other test compounds were determined in these cells by their ability to compete with the tracer leading to a reduction in the BRET signal. An overview of the assay is provided in (12).

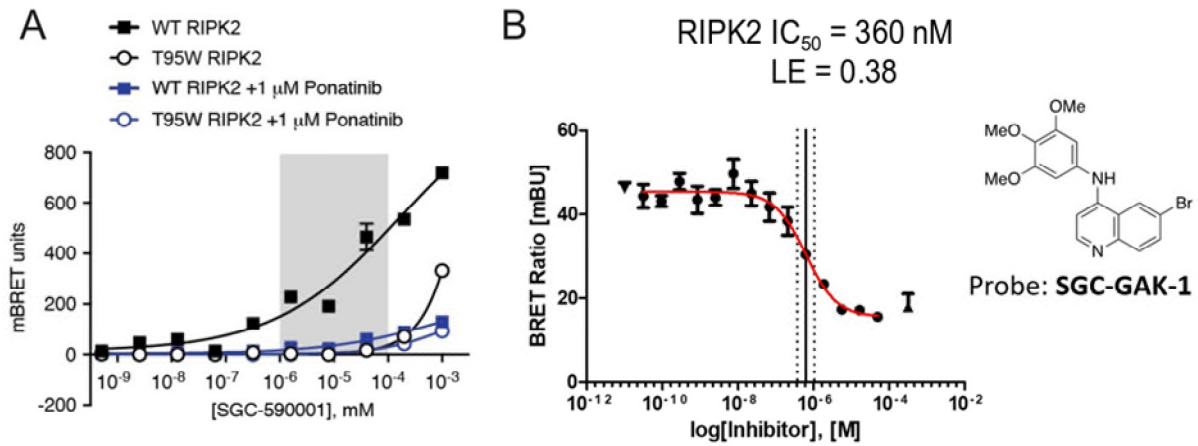

Fig. 6. Nanobret assay for RIPK2 in HEK293 cells. (**A**) Cells transfected with NanoLuc-RIPK2 were treated with serial dilutions of the SGC-590001 fluorescent probe to establish a window for Nanobret measurement. Signal was inhibited by 1 μM ponatinib (grey box indicates range of ponatinib concentrations explored). Resistance to ponatinib could be achieved by introduction of the RIPK2 T95W 'gatekeeper' mutation in the kinase hinge region. (**B**) Example IC_{50} measurement for RIPK2 inhibition by the GAK1 kinase chemical probe SGC-GAK1.

Assays of RIPK2 signalling

Inhibition of RIPK2 activation upon NOD2 stimulation with bacterial peptidoglycans

Stimulation of NOD2-expressing HEK293 cells with L18-MDP (a lipidated muramyl dipeptide with enhanced potency) caused a rapid increase in endogenous pSer176-RIPK2 (autophosphorylation) that could be blocked by small molecule inhibitors. Blocking RIPK2 activity prevented the subsequent degradation of IκBα, which is required for activation of NFκB (**Fig. 7**).

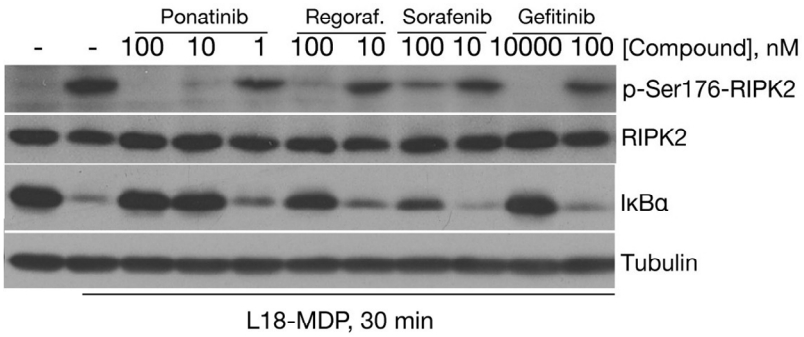

Fig. 7. Inhibition of RIPK2 activation in HEKBlue cells. Cells pretreated with inhibitor were stimulated with 1 μg/mL L18-MDP. Changes in RIPK2 phosphorylation and IκBα abundance after 30 mins were analyzed by Western blotting. Levels of tubulin and total RIPK2 were used as loading controls.

Small molecule inhibition of RIPK2 ubiquitination

Stimulation of NOD2 by MDP leads to rapid ubiquitination of RIPK2 by XIAP within 45 mins, a process required for downstream signalling. We analyzed this step in human monocytic THP-1 cells. Pre-treatment with ponatinib interfered with L18-MDP-induced RIPK2 ubiquitination in a dose-dependent manner. Concentrations as low as 5-10 nM reduced the extent and length of Ub-modified RIPK2, while RIPK2 ubiquitination was completely blocked at concentrations of 25 nM or higher (**Fig. 8**).

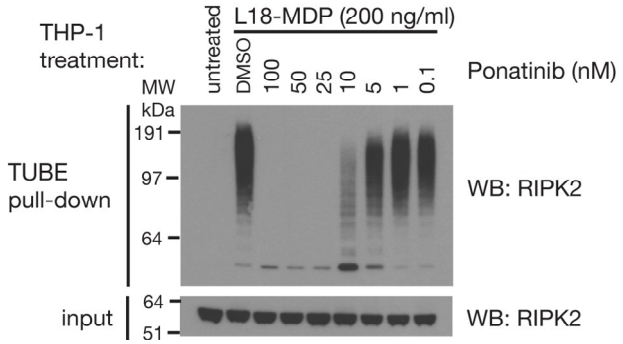

Fig. 8. Inhibition of RIPK2 ubiquitination in THP-1 cells. Cells were pretreated with kinase inhibitor or DMSO for 30 minutes and stimulated with 200 ng/mL L18-MDP. Ubiquitinated proteins were isolated using TUBE reagent and analysed by immunoblotting.

Assays showing RIPK2 catalytic activity is dispensable for NOD2-dependent inflammatory signalling

Ubiquitination and NF-κB signalling of kinase-dead RIPK2 mutants

U2OS/NOD2 RIPK2 KO cells were used to test the requirement for RIPK2 catalytic activity. Cells were reconstituted with either WT or kinase-dead RIPK2 mutants. Upon NOD2 stimulation with L18-MDP (200 ng/ml, 1 h) all variants of RIPK2 were ubiquitinated to a similar extent showing that RIPK2 catalytic activity was dispensable for this activation step. Ubiquitination of kinase-dead RIPK2 was also accompanied by the downstream destruction of IκBα which allows for NF-κB signalling (**Fig. 9**). Importantly, the ubiquitination of kinase-dead RIPK2 was still inhibited by ponatinib. These results suggested that efficacious RIPK2 kinase inhibitors might work through blocking XIAP binding and ubiquitination of RIPK2 rather than by blocking RIPK2 catalytic activity.

To quantify NF-κB signalling we used a dual luciferase NF-κB reporter assay in HEK293FT cells. NF-κB signalling was observed for both WT and kinase-dead RIPK2 variants and was inhibited by ponatinib consistent with the RIPK2 ubiquitination assay results. As ponatinib is a highly promiscuous kinase inhibitor we engineered a T95W gatekeeper mutation into all RIPK2 constructs to make them drug resistant (evidenced in **Fig. 6**). Kinase-dead RIPK2 mutants with the T95W mutation were still active in the NF-κB reporter assay, but were now unaffected by ponatinib confirmating that the signalling was specific to RIPK2 (**Fig. 9**).

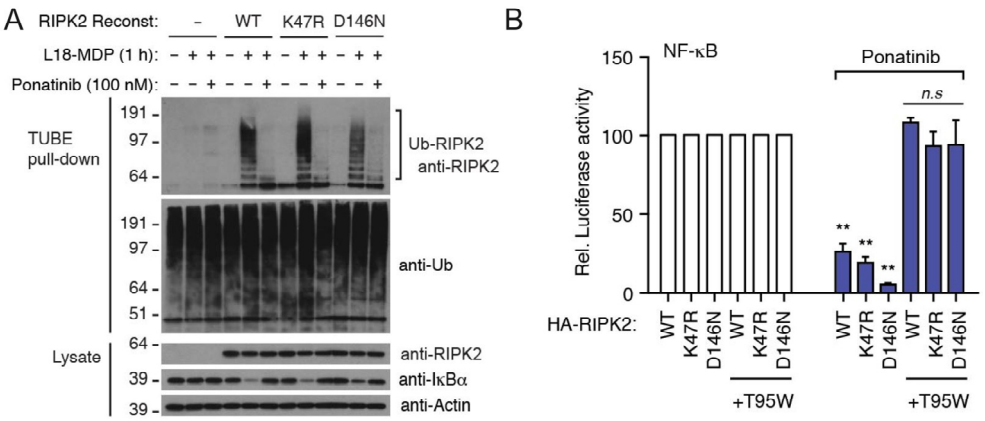

Fig. 9. Kinase inhibitors block NOD2-dependent inflammatory signalling from kinase-dead RIPK2 mutants. (**A**) U2OS/NOD2 RIPK2 KO cells were reconstituted with RIPK2 variants or empty vector. Stimulation with L18-MDP led to ubiquitination of all RIPK2 variants that was inhibited by ponatinib. (**B**) Signalling from WT and kinase-dead HA-RIPK2 constructs was measured in HEK293FT cells using a dual luciferase NF-κB reporter assay. Cells were treated with DMSO or ponatinib (200 nM, 24 h) as indicated. Relative luciferase activity in ponatinib-treated samples is shown relative to the activity in the corresponding HA-RIPK2 transfected sample not treated with inhibitor. Data represent mean ±SEM (n =4 independent experiments).

Assays of XIAP binding to RIPK2

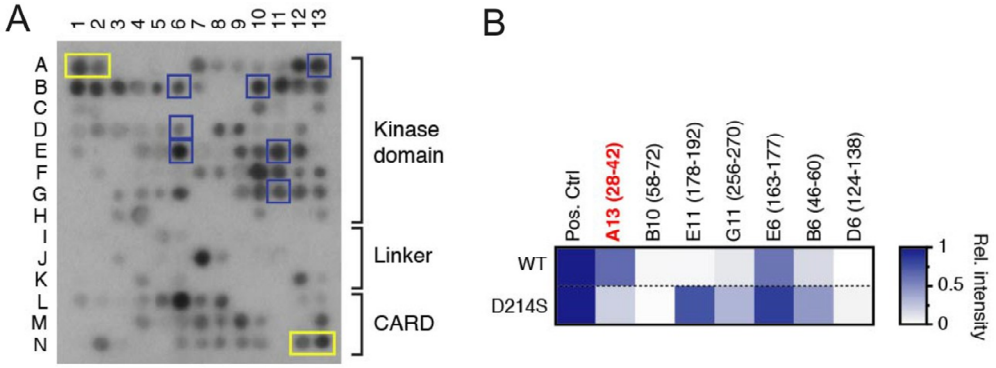

Fig. 10. Mapping of the XIAP-interacting surface on RIPK2. (**A**) SPOT synthesis 15-mer peptide array spanning the RIPK2 sequence and probed with 6xHis-GST-BIR2 domain protein. Bound protein by immunoblotting with anti-His antibody. (**B**) Quantification performed using ImageJ software for selected peptides reprinted in triplicate and probed with either WT or D214S mutant XIAP BIR2 domain. Peptide A13 (red labelling) showed specific binding to WT XIAP.

SPOT synthesis peptide array mapping of the XIAP-binding site on RIPK2

The XIAP BIR2 domain mutation D214S causes the immunodeficiency syndrome XLP2 (X-linked lymphoproliferative syndrome type-2) and has been shown to abolish XIAP binding to RIPK2. To map the corresponding XIAP-interaction surface on RIPK2, a SPOT synthesis peptide array was prepared spanning the entire sequence of RIPK2 with overlapping 15 a.a. peptides. Probing this array with 6xHis-GST-BIR2 protein identified seven putative interacting peptides in the kinase domain of RIPK2 (**Fig. 10A**). These peptides were reprinted in triplicate and further probed with either WT or D214S mutant BIR2 domain protein. A WT-specific interaction was observed for peptide A13 (RIPK2 residues 28-42) corresponding to the β2-β3 region of the kinase N-lobe (**Fig. 10B**).

RIPK2 kinase domain β2-β3 loop residues R36 and R41 appear critical for XIAP interaction

Alanine or leucine-scanning mutagenesis of RIPK2 a.a. 28-42 using the SPOT arrays identified R36 and R41 (β2-β3 loop) as the most critical residues for XIAP interaction (data not shown). To test this, we reconstituted RIPK2 KO U2OS/NOD2 cells with RIPK2 mutants R36L and/or R41L and performed a GST pull down with recombinant GST-BIR2-XIAP. Indeed, mutation of these residues impaired the interaction of RIPK2 with the XIAP BIR2 domain consistent with the SPOT array data (**Fig. 11A**).

Together these data suggest that the basic patch formed by RIPK2 R36/R41 in the kinase N-lobe β2-β3 loop mediates XIAP binding via a direct, electrostatic interaction with the acidic patch formed by E211, D214, E219 in the BIR2 IBM (IAP-binding motif) groove (**Fig. 11B**). The acidic pocket on the XIAP BIR2 domain is also the site of interaction of smac-mimetic small molecules that antagonise XIAP function.

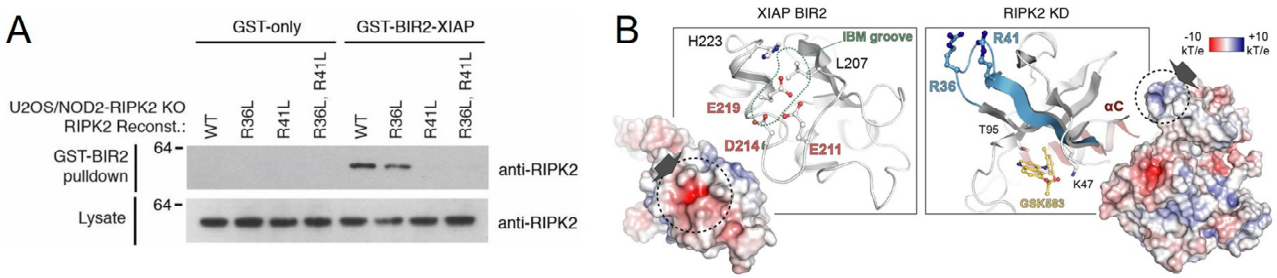

Fig. 11. RIPK2 residues R36 and R41 are critical for XIAP binding. (**A**) Pulldown of RIPK2 variants from U2OS/NOD2 cell lysates using recombinant GST-BIR2-XIAP protein. (**B**) Putative interaction surfaces (dashed borders) on XIAP BIR2 domain (left, PDB 1C9Q) and RIPK2 kinase domain (right, PDB 5AR2).

Chemical Matter

1. FDA-approved inhibitors ponatinib, regorafenib, sorafenib
2. Type II inhibitor CSR35 and fragments
3. Type I inhibitor CSLP series

Inhibitor co-crystal structures

Co-crystal structures were solved for three inhibitors: ponatinib, CSR35 and CSLP18 (**Fig. 12**).

Findings from the ponatinib complex

We identified ponatinib as a RIPK2 inhibitor with an EC_{50} of 0.8 nM in HEKBlue cells. Ponatinib is a highly promiscuous type II inhibitor developed against drug-resistant mutants of the Abl kinase. It is approved by the US FDA for late stage leukaemia. Due to its severe adverse effects, ponatinib is not suitable for use in chronic indications, such as those potentially involving RIPK2. Nonetheless, the co-crystal structure of ponatinib revealed that the back pocket created by the DFG-out configuration of RIPK2 was increased in size relative to other kinases due to the presence of RIPK2 Ala73 (**Fig. 13**).

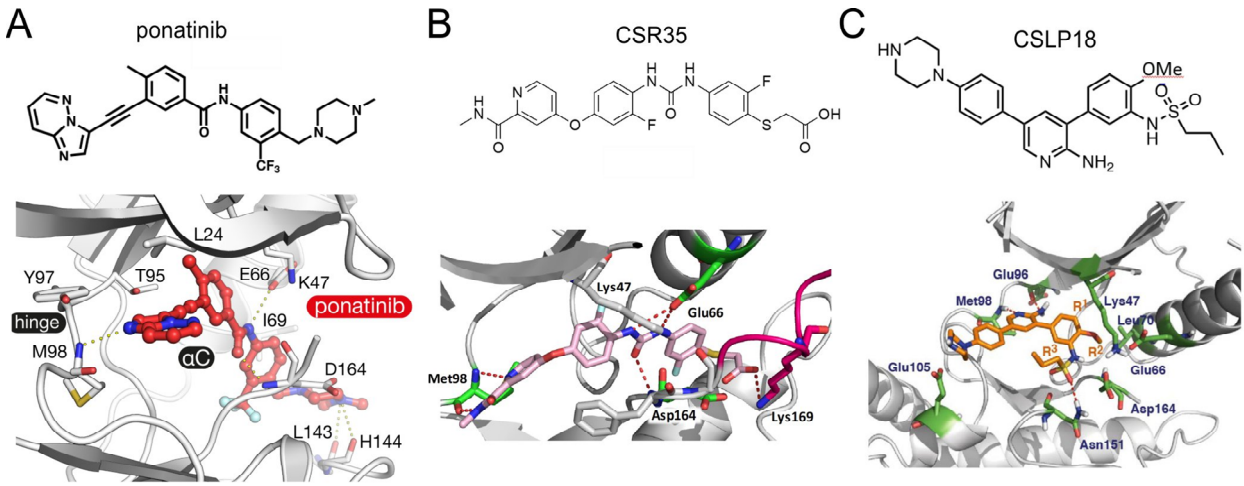

Fig. 12. Crystal structures of RIPK2-inhibitor complexes. (**A**) Ponatinib complex (4C8B, 2.75 Å). (**B**) CSR35 complex (6ES0, 2.38 Å). (**C**) CSLP18 complex (6FU5, 3.26 Å).

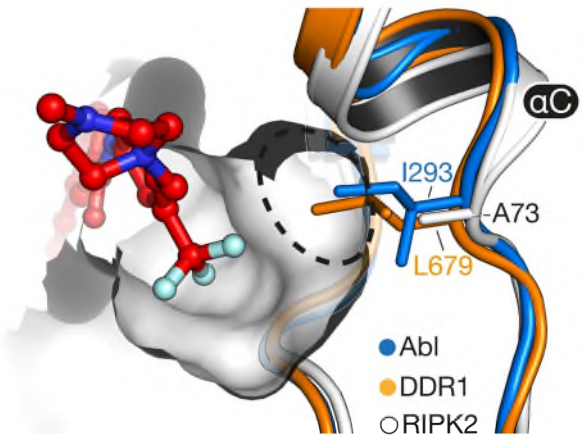

Fig. 13. Extended back pocket in RIPK2. The trifluoromethyl group of ponatinib occupies the hydrophobic pocket vacated by the inverted DFG motif. Here the pocket is greatly enlarged in RIPK2 due to the presence of Ala73 (αC), whereas nearly all kinases contain a bulky side chain at this position, such as Leu70 in RIPK1.

Thus, there may be opportunities for the development of larger RIPK2-selective molecules that would be sterically restricted from binding to the wider kinome.

Findings from the CSR35 complex

The type II inhibitor CSR35 was modified from the regorafenib scaffold to find a new interaction with the activation loop of RIPK2 as a strategy to explore novel kinase regions for improved inhibitor selectivity. Our co-crystal structure of CSR35 with RIPK2 revealed a new ionic interaction between the inhibitor's carboxylic acid and the side-chain of Lys169. Unfortunately, the inhibitory potency was reduced some 50-fold suggesting further chemistry would be required to optimise this approach (**Fig. 14**). Notably, fragments CSR35F1 and CSR35F2 targeting the allosteric back pocket also inhibited RIPK2 suggesting potential for investigation of type III inhibitors that engage the activation loop (**Fig. 14**).

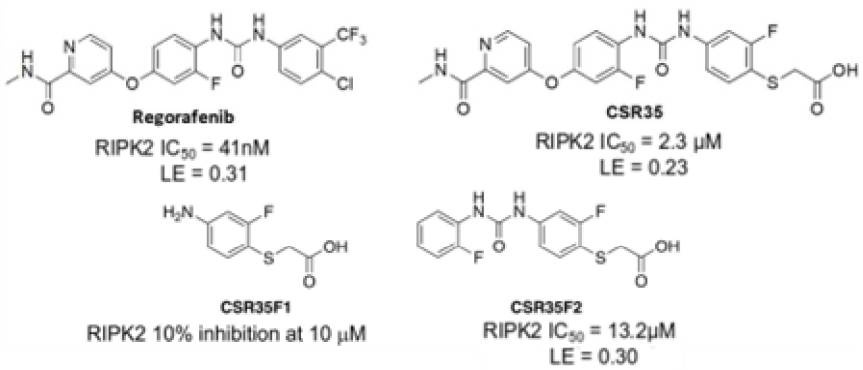

Fig. 14. Chemical structures and IC_{50} values for RIPK2 inhibitors derived from regorafenib.
IMPORTANT: Please note that the existence of small molecules within this TEP only indicates that chemical matter can bind to the protein in a functionally relevant pocket. As such, these molecules should not be used as tools for functional studies of the protein unless otherwise stated as they are not sufficiently potent or well-characterised to be used in cellular studies. The small molecule ligands are intended to be used as the basis for future chemistry optimisation to increase potency and selectivity and yield a chemical probe or lead series.

Findings from the CSLP inhibitor series

The CSLP inhibitor series derives from our previous work on ALK2 kinase inhibitors (**Fig. 15**)(13). Compounds such as LDN-214117 showed potent inhibition of RIPK2 (IC_{50} = 50 nM) as well as promising selectivity against the human kinome.

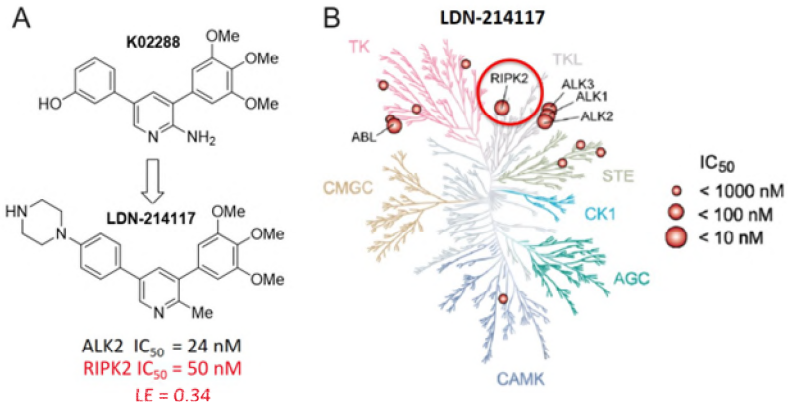

Fig. 15. Discovery of pyridine derivatives as RIPK2 inhibitors. (**A**) Chemical scaffolds of early derivatives. (**B**) Kinome selectivity profile of LDN-214117 (Nanosyn, >200 kinases).

As shown previously in **Fig.5**, a significant number of inhibitors in the CSLP series displayed potent inhibition of RIPK2 enzymatic activity, but only some of these were potent in cells, notably CSLP37 and CSLP43 (**Fig. 16**).

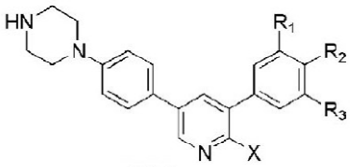

CSLP

Compd ID	X	R¹	R²	R³	IC_{50} (nM)		
					In vitro kinase	Cellular activity	
					RIPK2 ADPGlo	HEKBlue NOD2	nanoBRET RIPK2 binding
CSLP43	NH_2	OMe	OMe	-$NHSO_2{}^nPr$	19.9 ±0.8	1.3 ±0.4	10.1 ±3.8
CSLP37	NH_2	F	OMe	-$NHSO_2{}^nPr$	16.3 ±4.6	26.3 ±3.7	36.3 ±20.2
CSLP18	NH_2	H	OMe	-$NHSO_2{}^nPr$	31.6 ±8.7	476.0 ±96.7	577.6 ±34.1
CSLP38	NH_2	F	H	-$NHSO_2{}^nPr$	39.1 ±1.5	740.3 ±60.7	166.8 ±19.0
CSLP48	NH_2	H	OH	-$NHSO_2{}^nPr$	53.5 ±5.7	>5,000	1231.3 ±344.5
CSLP53	Me	F	OMe	-$NHSO_2{}^nPr$	1,414.5 ±311.6	2,556.5 ±252.8	>10,000
CSLP55	NH_2	F	OMe	OMe	39.1 ±3.9	595.1 ±69.6	194.6 ±47.1

Fig. 16. SAR of pyridine derivatives in the CSLP series comparing in vitro kinase (ADP-Glo) and cellular assays (HEKBlue NF-κB reporter and RIPK2 nanoBRET).

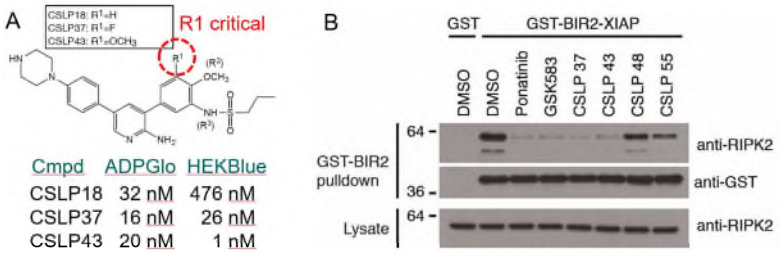

Fig. 17. CSLP37 and CSLP43 inhibit XIAP binding and HEKBlue NF-κB reporter. (**A**) Mini-SAR highlighting the importance of a larger substituent at the R1 position to achieve potency in HEKBlue cells. (**B**) Effective RIPK2 inhibitors such as CSLP37 and CSLP43 block binding of XIAP.

Specific comparison of CSLP18, CSLP37 and CSLP43 revealed a striking dependence of the cellular activity of these inhibitors on the size of the substituent at the R1 position (**Fig. 17A**). CSLP37 and CSLP43 blocked XIAP binding, whereas CSLP48 and CSLP55, which lacked cellular potency, failed to block XIAP binding (**Fig. 17B**). Structural modelling suggested that the critical R1 substituent fills the deep back pocket besides the Thr95 gatekeeper residue in the kinase hinge region (**Fig. 18**). This pocket lies adjacent to and below the mapped interaction surface for XIAP. Other efficacious RIPK2 inhibitors such as ponatinib, fill the same pocket. Thus, one can envision that inhibitor interactions at this site may interfere with the preferred β2-β3 loop conformation for XIAP interaction.

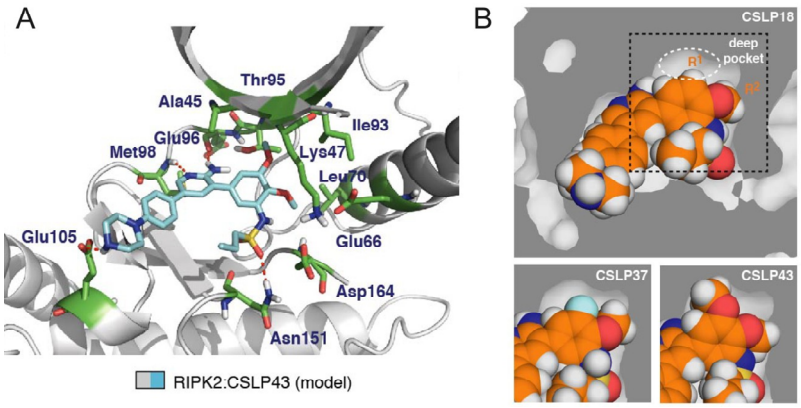

Fig. 18. CSLP43 fills a deep pocket by the gatekeeper Thr95. (**A**) Model of the RIPK2-CSLP43 complex. (**B**) Spacefill models of CSLP series inhibitors highlighting their occupation of the deep back pocket.

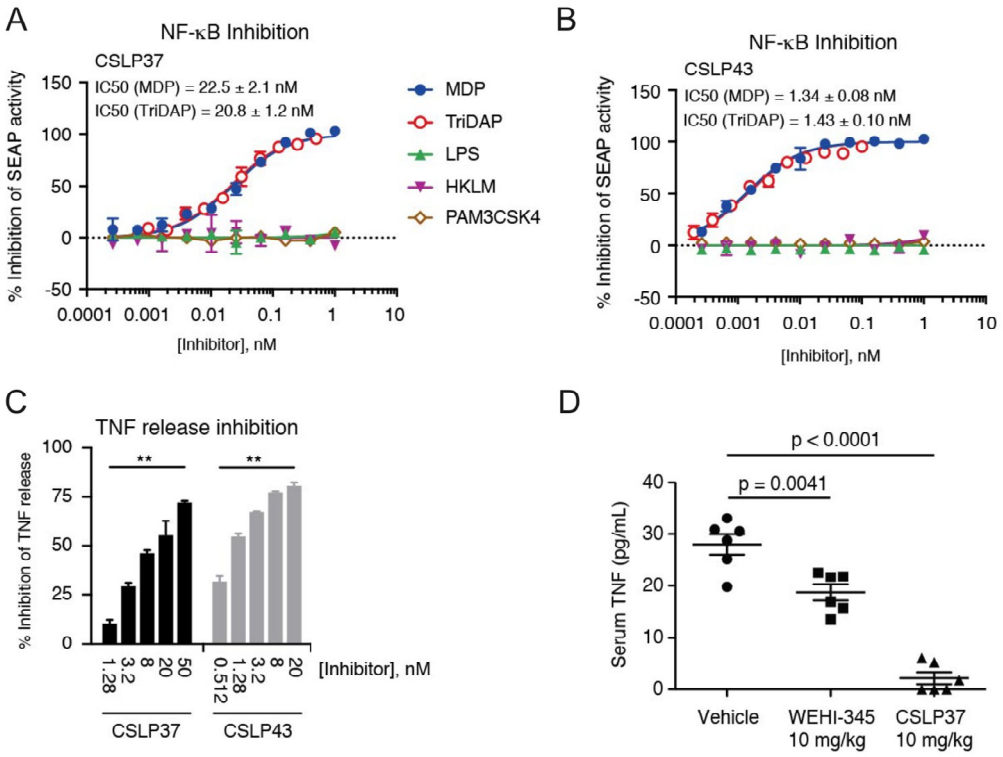

Fig. 19. Inhibitory activities of CSLP37 and CSLP43. Inhibition of the NF-κB SEAP reporter by (**A**) CSLP37 and (**B**) CSLP43 in THP1-Blue™ NF-κB cells (Invivogen) treated with either MDP (10 µg/mL), TriDAP (10 µg/mL), E. coli LPS (10 ng/mL), HKLM (1x10^7 cells/mL or Pam3CSK4 (10 ng/mL). Data represent mean ± SEM (n = 3). (**C**) ELISA measurement of TNF release from RAW264.7 cells treated with MDP (10 µg/mL, 24 h) and CSLP compounds. (**D**) Inhibition of MDP-elicited TNF release in vivo. Mice (n=6 per group) were administered i.p. with 10 mg/kg of WEHI-345 or CSLP36 30 min prior to ip injections of 100 µg/mouse of MDP. After 4 h, blood was collected by cardiac puncture and circulating levels of TNF were analyzed by ELISA.

CSLP37 and CSLP43 selectively inhibit NOD responses in cells and display potent activity in vivo

The inhibitory properties of CSLP37 and CSLP43 experiments are summarised in **Fig. 19**. In human THP1 monocytes containing an NF-κB-SEAP reporter, CSLP37 and CSLP43 selectively blocked RIPK2 signalling from NOD1 (TriDAP stimulation) and NOD2 (MDP stimulation), with no detected effect on TLR1, TLR2 and TLR4 responses (LPS, HKLM, or Pam3CSK4 stimulation, **Figure 4A-B**). CSLP37 and CSLP43 also blocked the downstream release of TNF in mouse RAW264.7 macrophages with similar IC_{50} values to those in the previous NOD2/HEKBlue assay. Finally, CSLP37 could effectively block TNF release in a MDP-challenge model in vivo.

Antibodies

The following antibodies from were used from Santa Cruz Biotechnology: anti-RIPK2 mouse monoclonal (clone A-10, sc-166765), goat polyclonal (sc-8610, discontinued) and rabbit polyclonal (H-300, sc-22763, discontinued). The phospho-specific antibody rabbit anti-phospho-Ser176-RIPK2 was obtained from Cell Signaling.

CRISPR/Cas9 reagents

RIPK2 KO U2OS/NOD2 cells were prepared by our collaborator Mads Gyrd-Hansen using the CRISPR/Cas9 KO plasmids (containing gRNA, Cas9, and EGFP reporter) from Santa Cruz Biotechnology (Hrdinka et al. manuscript under review). Additionally, CRISPR/Cas9 reagents targeting human RIPK2 have been published by others (14) and are available from Addgene (plasmids #76912, #76911, #76910).

Future plans

A manuscript (Hrdinka et al.) reporting that RIPK2 catalytic activity is dispensible for NOD2-RIPK2 pro-inflammatory signalling is currently under review. Further development of the CSLP inhibitor series is in progress in collaboration with Alexei Degterev and Greg Cuny with potential to generate a highly selective and potent chemical probe.

Collaborations

Chemistry partner: Gregory D. Cuny (University of Houston)
Kinase assays: Alexei Degterev (Tufts University)
XIAP and ubiquitination assays: Mads Gyrd-Hansen (University of Oxford)
FACS assays: Holm H. Uhlig (University of Oxford)

CONCLUSION

Genetic variants in NOD2 and RIPK2 associated with increased signalling through the NOD2-RIPK2 pathway are implicated in auto-immune and auto-inflammatory diseases. RIPK2 has therefore emerged as a promising therapeutic target, but its targeting has been complicated by the lack of correlation between inhibitor potencies in in vitro kinase assays and in cellular assays. Here we rationalise this effect by demonstrating that the catalytic activity of RIPK2 is dispensable for pro-inflammatory signalling through the NOD2-RIPK2 pathway.

Our data further reveal that RIPK2 activity is critically dependent on binding of the XIAP E3 ligase to the kinase N-lobe of RIPK2, specifically at a basic patch formed by the β2-β3 loop. Efficacious RIPK2 inhibitors with potency in cells appear to fill a deep back pocket in the ATP-binding pocket by the gatekeeper position which lies proximal to the XIAP interaction surface. These inhibitors block XIAP interaction and XIAP-mediated ubiquitination of RIPK2. Finally, we report CSLP37 and CSLP43 as low nanomolar inhibitors of RIPK2 with inhibitory activity both in cells and in vivo.

Subsequent to this TEP, GSK published the development of GSK583 and compound 7 as novel RIPK2 inhibitors with exquisite selectivity and potency that further supported the potential of RIPK2 as a therapeutic target (15).

TEP IMPACT

Publications arising from this work:

Parts of this work have been published in the following:

- Suebsuwong C, Dai B, Pinkas DM, Duddupudi AL, Li L, Bufton JC, Schlicher L, Gyrd-Hansen M, Hu M, Bullock AN, Degterev A, Cuny GD. (2020). Receptor-interacting protein kinase 2 (RIPK2) and nucleotide-binding oligomerization domain (NOD) cell signaling inhibitors based on a 3,5-diphenyl-2-aminopyridine scaffold. Eur J Med Chem. 200:112417.
- Hrdinka M, Schlicher L, Dai B, Pinkas DM, Bufton JC, Picaud P, Ward JA, Rogers C, Suebsuwong C, Nikhar S, Cuny GD, Huber KVM, Filippakopoulos P, Bullock AN, Degterev A, Gyrd-Hansen M. (2018). Small molecule inhibitors reveal an indispensable scaffolding role of RIPK2 in NOD2 signaling. EMBO J.
- Suebsuwong C, Pinkas DM, Ray SS, Bufton JC, Dai B, Bullock AN, Degterev A, Cuny GD. (2018). Activation loop targeting strategy for design of receptor-interacting protein kinase 2 (RIPK2) inhibitors. Bioorg Med Chem Lett. 28(4):577-583.
- Bullock AN, Degterev A. (2015). Targeting RIPK1,2,3 to combat inflammation. Oncotarget. 6(33):34057-8.
- Canning P, Ruan Q, Schwerd T, Hrdinka M, Maki JL, Saleh D, Suebsuwong C, Ray S, Brennan PE, Cuny GD, Uhlig HH, Gyrd-Hansen M, Degterev A, Bullock AN. (2015). Inflammatory Signaling by NOD-RIPK2 Is Inhibited by Clinically Relevant Type II Kinase Inhibitors. Chem Biol. 22(9):1174-84.

FUNDING INFORMATION

The work performed at the SGC has been funded by a grant from the Wellcome [106169/ZZ14/Z].

ADDITIONAL INFORMATION

Structure Files

PDB ID	Structure Details	Compound ID
4C8B	2.75 Å structure of the human RIPK2 kinase domain bound to ponatinib	PK005988d
6ES0	2.38 Å structure of the human RIPK2 kinase domain bound to CSR35	PK010729a
6FU5	3.26 Å structure of the human RIPK2 kinase domain bound to CLSP18	PK011996a

Materials and Methods

Protein Expression and Purification

Preparation of the Human RIPK2 kinase domain
Boundaries: residues 3-317 (WT) or 8-317 (R171C mutant)
Vector: pFB-LIC-Bse
Tag and additions: TEV-cleavable N-terminal hexahistidine tag
Expression cell: Sf9 insect cells

Bacmid DNA was prepared from DH10Bac cells and used to transfect Sf9 insect cells for the preparation of initial baculovirus. RIPK2 protein was expressed from infected Sf9 cells cultivated in InsectXpress medium (Lonza) for 48 hours at 27°C. Harvested cells were resuspended in lysis buffer (50 mM HEPES pH 7.4, 500 mM NaCl, 5 mM imidazole, 5% glycerol) supplemented 0.5 mM TCEP (tris(2-carboxyethyl)phosphine) and protease inhibitor cocktail set V (Calbiochem) at 1:1000 dilution. Cells were lysed using an Emulsiflex C5 homogeniser or by sonication, clarified by centrifugation, and the recombinant protein collected by nickel-affinity chromatography and eluted by imidazole. The tag was cleaved by TEV protease and RIPK2 protein either left untreated (heterogeneous 2-5 phosphorylations) or treated with lambda phosphatase overnight at 4°C. Further purification was performed on a Superdex 75 26/60 gel filtration column pre-equilibrated in 10 mM HEPES pH 7.4, 500 mM NaCl, 5% glycerol, 1 mM TCEP. When dephosphorylated the final protein was prone to aggregation and was therefore supplemented with 5 mM L-arginine, 5 mM L-glutamate and 2 mM DTT.

Preparation of the Human XIAP BIR2 domain
Boundaries: residues 124-242 (Wild type or D214S mutant)
Vector: pGTVL2
Tag and additions: TEV-cleavable N-terminal hexahistidine and GST tags
Expression cell: E. coli (BL21DE3) cells

The WT or mutated (D214S) BIR2 domain of XIAP was expressed in E. coli (BL21DE3) cells as a fusion protein with N-terminal 6xHis and GST tags. Protein expression was induced with 0.5 mM IPTG for 16 h at 16 °C. Cells were lysed in binding buffer (50 mM HEPES pH 7.5, 500 mM NaCl, 5% Glycerol, 10 mM Imidazole, 0.5 mM TCEP) using an Emulsiflex C5 homogeniser or by sonication. After centrifugation at 4 °C the extract was loaded onto a 5 mL HisTrap FF column, washed and eluted with elution buffer (50 mM HEPES pH 7.5, 500 mM NaCl, 5% Glycerol, 250 mM Imidazole. Further clean up was performed on a gel filtration column HiLoad 26/600 Superdex 75 pg (GE Healthcare Life Sciences) equilibrated in 50 mM HEPES pH 7.5, 300 mM NaCl, 5% Glycerol, 0.5 mM TCEP. Collected fractions corresponding to monomeric form of the recombinant protein were frozen in liquid nitrogen, stored at -80 °C and used for probing of peptide array membranes. Alternatively, cells were lysed using BugBuster protein extraction reagent (#70921, Merck Millipore) and XIAP protein purified in batch using Glutathione Sepharose Fast Flow beads (GE Healthcare Life Sciences, Little Chalfont, UK). After 4 h, the beads were washed with PBS and directly used for GST pull-down experiments or stored at 4 °C.

Structure Determination

RIPK2 kinase domain with ponatinib (PDB: 4C8B)

Dephosphorylated RIPK2 R171C was concentrated to 3.7 mg/mL and ponatinib added to a slight molar excess. Crystals were grown using the vapour-diffusion technique in 150 nL sitting drops containing 75 nL protein and 75 nL of a reservoir solution containing 0.1 M ammonium citrate and 16% (w/v) PEG3350 at 20°C. Crystals were cryo-protected by addition of 25% ethylene glycol before being vitrified in liquid nitrogen. Diffraction data were collected at 100K on Diamond Light Source beamline I04. Data were indexed and integrated using XDS (16) and scaled using AIMLESS (17) in the CCP4 suite of programs (18). Phases were identified using molecular replacement in PHASER (19) and the PDB 3PPZ as a search model. Structures were built using PHENIX.AUTOBUILD (20) and then refined and modified using alternate rounds of REFMAC5 (21) and COOT (22). TLS groups were determined using the TLSMD server (23). The refined structure was validated with MolProbity (24).

RIPK2 kinase domain with CSR35 (PDB: 6ES0)

Phosphorylated WT RIPK2 was concentrated to 10 mg/mL in the presence of 2 mM CSR35 and 1% DMSO final concentration. After 10 min incubation, the mix was filtered to 0.22 µm. Crystals were grown using the vapour-diffusion technique in 150 nL sitting drops containing 50 nL protein and 100 nL of a reservoir solution containing 25% PEG Smear (low MW), 0.1 M MES pH 6.5, 0.05 M magnesium acetate, 0.05 M magnesium chloride at 20°C. Crystals were cryo-protected by addition of 25% ethylene glycol before being vitrified in liquid nitrogen. Diffraction data were collected at 100K on Diamond Light Source beamline I04. Data were indexed and integrated using XDS and scaled using AIMLESS. Phases were identified using molecular replacement in PHASER and the PDB ID: 4C8B as a search model. Structures were built using PHENIX.AUTOBUILD and then refined and modified using PHENIX.REFINE and COOT. The refined structure was validated with MolProbity and the atomic coordinate files deposited in the Protein Data Bank.

RIPK2 kinase domain with CSLP18 (PDB: 6FU5)

Phosphorylated WT RIPK2 was concentrated to 10 mg/mL in the presence of 2 mM CSLP18 and 1% DMSO final concentration. After 10 min incubation, the mix was filtered to 0.22 µm. Crystals were grown using the vapour-diffusion technique in 150 nL sitting drops containing 100 nL protein and 50 nL of a reservoir solution containing 0.2 M potassium formate and 20% (w/v) PEG3350 at 20°C. Crystals were cryo-protected by addition of 25% ethylene glycol before being vitrified in liquid nitrogen. Diffraction data were collected at 100K on Diamond Light Source beamline I04 using 0.9795 Å light. Data were indexed and integrated using XDS and scaled using AIMLESS. Phases were identified using molecular replacement in PHASER and the PDB ID: 4C8B as a search model. Structures were built using PHENIX.AUTOBUILD and then refined and modified using PHENIX.REFINE and COOT. The refined structure was validated with MolProbity and the atomic coordinate files deposited in the Protein Data Bank.

Assays

Analytical gel filtration

A Superdex 200 10/300 GL gel filtration column (GE healthcare) was attached to an Akta Purifier FPLC system (GE healthcare) and equilibrated in gel filtration buffer (50mM HEPES pH7.5, 150mM NaCl, 2mM TCEP). 500 µL of RIPK2 at 50 µM was injected onto the column, which was run at 0.5 mL/min and monitored using absorbance at 280 nm. The retention volume of RIPK2 was compared with the retention volumes of a set of gel filtration standards (Bio-Rad laboratories), which were run under the same conditions.

Thermal shift assay

A fluorescence-based thermal shift assay (differential scanning fluorimetry (DSF)) was performed as an initial screen to identify potential RIPK2 inhibitors. Ligands in this assay increase a protein's melting temperature (T_m

shift) by an amount proportional to their binding affinity. A solution of 2 µM RIPK2 protein in assay buffer (20 mM HEPES pH 7.4, 150 mM NaCl, 0.5 mM TCEP, 5% glycerol) was mixed 1:1000 with SYPRO Orange (Sigma). Compounds to be tested were added to a final concentration of 10 µM. 20 µL of each sample were placed in a 96-well plate and heated from 25 to 95°C. Fluorescence was monitored using a Mx3005P real-time PCR instrument (Stratagene) with excitation and emission filters set to 465 and 590 nm, respectively. Data were analysed with the MxPro software and curves fit in Microsoft Excel using the Boltzmann equation to determine the midpoint of thermal denaturation (T_m). Thermal shift values (ΔT_m) induced by inhibitor binding were calculated relative to control wells containing protein and 2.5% DMSO.

ADP-Glo in vitro kinase assays

For ADP-Glo (Promega) assays, 10 ng of RIPK2 was diluted in reaction buffer (40 mM Tris-HCl pH 7.5, 20 mM $MgCl_2$, 0.5 mM DTT, 0.01% BSA) supplemented with 50 µM ATP and 10-point dose range of inhibitors. Reactions were performed at room temperature for 1 hour. Reactions were performed in 5 µL total volume (5% final concentration of DMSO) and stopped by addition of 5 µL of ADP-Glo reagent for 40 min at room temperature. Luminescent signal was generated by addition of 10 µL of kinase detection reagent for 30 minutes at room temperature and determined using Victor3V platereader (Perkin Elmer). Specific signal was calculated by subtracting values in the wells without protein and inhibitor from the values in the test wells. Inhibition, % = ((specific signal (DMSO control) - specific signal (inhibitor))/ (specific signal (DMSO control))) x 100%. Non-linear regression to determine IC_{50} values was performed using Prism software (GraphPad).

NOD2-HEK-Blue activation assay

For nanoBRET experiments full length RIPK2 was cloned into pFC32K-Nluc (Promega, Madison, WI). HEK-Blue hNOD2 cells (Invivogen) were maintained in DMEM medium (Fisher) supplemented with 10% FBS (Sigma) and 1% antibiotic-antimycotic mix (PSA) (Invitrogen) as well as Normocin (100 µg/mL), Blasticidin (30 µg/mL) and Zeocin (100 µg/mL). Cells ($7.5x10^3$ cells/mL) were seeded into clear 96 well plates and allowed to attach for 48 h. On the day of the experiment, media was changed to 100 µl of QUIATI-Blue detection media (InvivoGen). Inhibitors were diluted and added in 0.5 µL DMSO 15 min prior to the addition of 1 µg/mL L18-MDP (InvivoGen). After 8-10 hours, absorbance at 620 nM was determined using Victor3V plate reader (Perkin Elmer). Values of empty media were subtracted from all experimental samples. Resulting specific signal values were used to calculate inhibition, % = (1-(control (DMSO, L18-MDP) – sample (compound, L18-MDP))/(control (DMSO, L18-MDP)-control (DMSO)))*100. EC_{50} values were determined using non-linear regression in the Prism software package (GraphPad).

RIPK2 nanoBRET assay

HEK293 cells were cultured in DMEM GlutaMax (Gibco) supplemented with 10 % (v/v) FBS (Sigma-Aldrich) and 1 % (v/v) Penicillin-Streptomycin (Gibco). Cells were transiently transfected with a NanoLuc-RIPK2 construct together with Transfection Carrier DNA (Promega). After 20 h, transfected cells were plated at 2×10^5 cells/mL into a white 384-well assay plate (Corning, Corning, NY), treated with 0.25 µM fluorescent tracer SGC-590001, and incubated with inhibitor or DMSO control for 3 h. After addition of Nano-Glo Substrate (Promega) and Extracellular NanoLuc Inhibitor (Promega), BRET ratios (450 nm and 610 nm) were determined using a PHERAstar FSX plate reader (BMG Labtech). The preparation of SGC-590001 and further details of the assay were described previously (12).

NanoBRET inhibition assay

Inhibitor IC_{50} measurements were alternatively performed in HEKBlue cells. Cell density was adjusted to $2x10^5$ cells/mL. 100x NanoBRET In-cell Kinase Tracer (Promega) was diluted to 20x in phenol red-free Opti-MEM supplemented with 12.5 mM HEPES (Thermo Fisher Scientific) and 31.25% PEG-400 (Sigma-Aldrich). 10x inhibitor stocks in Opti-MEM were prepared by diluting DMSO stocks. For the assay, 11.9 µL cells/well were seeded into a while low volume 384 well plate (Corning) and mixed with 0.7 µL 20x tracer and 1.4 µL 10x inhibitors, followed by incubation for 2 h at 37°C. 3x substrate mix was prepared by adding NanoBRET Nano-

Glo substate (Promega) (1:166 dilution) and extracellular NanoLuc Inhibitor (Promega, 1:500 dilution) into Opti-MEM media. 7 µL of 3x substrate mix was added into each well with the cells. Plate was mixed on a rotary shaker for 15 sec at 500 rpm. Emission was determined using Victor3V plate reader at 460 nm for donor (NanoLuc) and 610 nm for acceptor (tracer). NanoBRET ratios were calculated as [($Acceptor_{sample}$ / $Donor_{sample}$) – ($Acceptor_{no\ tracer\ control}$/$Donor_{no\ tracer\ control}$)] x 1000 and used for non-linear regression to calculate IC_{50} values.

Immunoblot analysis

HEK-Blue cells were seeded into 10 cm^2 dishes to achieve 80-90% confluency after 48 hr. Cells were pre-treated with inhibitors for 30 min and stimulated with L18-MDP for 30 min. Cells were lysed in RIPA buffer supplemented with PMSF), briefly sonicated and spun in a 4°C centrifuge at 14,000 rpm for 15 min to collect lysates. Protein concentrations were measured using 660 nM protein assay reagent (Pierce). Equal amounts of proteins were separated using 8-10% SDS-PAGE, followed by overnight incubations with antibodies according to the manufacturer's recommendations. Commercially available antibodies included mouse anti-RIPK2 (clone A-10 from Santa Cruz), mouse anti-Ubiquitin (clone Ubi-1, Imgenex), rabbit anti-phospho-Ser176-RIPK2 (Cell Signaling), mouse anti-α-tubulin (clone DM1A, Cell Signaling), mouse anti-IκBα (clone L35A5, Cell Signaling), and anti-actin (clone MAB1501, Millipore). The NOD1 ligand Tri-DAP, NOD2 ligands L18-MDP and MDP and TLR2 ligand Pam3CSK4 were purchased from Invivogen, LPS (E.coli 0111:B4) from Sigma and recombinant TNF from Enzo.

Analysis of RIPK2 ubiquitination in THP-1 cells

Human monocytic THP-1 cells were cultured in RPMI 1640 medium (Gibco) supplemented with 10% FBS and Penicillin / Streptomycin at density 0.6 −1.0 million cells per mL.. Cells were pretreated with kinase inhibitor or DMSO for 30 minutes and stimulated with 200 ng/mL L18-MDP for 45 mins to 4 hr. The ubiquitin conjugates were purified using GST-Tandem Ubiquitin Binding Entities (TUBE; (25)). Briefly, treated THP-1 cells ($6–10\times10^6$) were washed with PBS and lysed in 400 µL of ice-cold lysis buffer (20 mM Na_2HPO_4, 20 mM NaH_2PO_4, 1% NP-40, 2 mM EDTA) containing 50 µg/ml of GST-TUBE1 (Lifesensors, Malvern, PA) on ice for 30 minutes. Cleared lysates were incubated with Glutathione Sepharose 4B resin (Amersham) with agitation at 4°C overnight. The beads were washed four times with PBS-Tween (0.1%) and the bound proteins were released by heating the beads in reducing SDS sample buffer. The samples were subjected to immunoblotting using mouse anti-Ubiquitin (clone Ubi-1, Imgenex) and anti-RIPK2 antibodies.

Generation of RIPK2 KO U2OS/NOD2 cells and reconstitution with RIPK2 variants

NOD2-expressing U2OS-Flp-In™ T-REx™ (U2OS/NOD2) cells have been described previously (Fiil et al., 2013) and were cultured in DMEM GlutaMax (Gibco) supplemented with 10% (v/v) FBS (Sigma) and 1% (v/v) Penicillin-Streptomycin (Gibco) and transfected using Fugene 6 (Promega). U2OS/NOD2 cells express doxycycline (DOX)-inducible HA-NOD2, but respond to L18-MDP without addition of DOX due to leakiness of the promoter (25). RIPK2 KO was generated using the CRISPR/Cas9 KO plasmids (containing gRNA, Cas9, and EGFP reporter) from Santa Cruz Biotechnology. These RIPK2 KO cells were then reconstituted retrovirally with WT RIPK2 or the kinase-dead RIPK2 mutants K47R or D146N (pBABE-Puro plasmids). All U2OS/NOD2 cells were cultured and stimulated in the absence of doxycycline unless otherwise indicated. The pcDNA3-HA-NOD2 expression vector was a gift to our collaborators from Dr G Nuñez (University of Michigan).

Dual luciferase NF-κB reporter assay

HEK293FT cells were co-transfected the NF-κB luciferase reporter construct pBIIX-luc and a thymidine kinase-renilla luciferase construct for normalization of transfection efficiency. Additionally, cells were co-transfected with WT or mutant HA-RIPK2 as required (pcDNA3-RIPK2-3xHA was a gift from T. Tenev/P. Meier). After 24-48 h, cells were lysed in 75 µL passive lysis buffer (Promega) and luciferase activity was measured on a FLUOstar Omega Microplate Reader (BMG LABTECH) using the Dual-Luciferase® Assay System (Promega). Where desired, cells were treated with DMSO or ponatinib (200 nM) 24 h before lysis.

SPOT synthesis peptide array

Cellulose-bound peptide arrays were prepared employing standard Fmoc solid phase peptide synthesis using a MultiPep-RSi-Spotter (INTAVIS, Köln, Germany) according to the manufacturer's method. Arrays were probed with WT or D214S mutant 6xHIS-GST-tagged BIR2 domain of XIAP produced in E. coli. Bound protein was detected using anti-His antibody HPR conjugated (diluted 1:15000) and the Pierce® ECL Western blotting Substrate (#32106, Thermo Fisher Scientific). Chemiluminescence was detected using Super RX films (FUJIFILM) and quantification performed using ImageJ software.

GST-BIR2-XIAP pull down of cellular RIPK2 variants

For GST pull-down experiments, U2OS/NOD2 were lysed in TBS lysis buffer containing 0.5% NP-40, cOmplete and PhosSTOP inhibitors (Roche). Cleared lysates were pretreated with kinase inhibitors or DMSO and incubated with GST-XIAP-BIR2 bound to Glutathione Sepharose at 4 °C overnight. Bound material was washed 3x with lysis buffer or PBS, eluted with 15 mM Glutathione in PBS and analyzed by immunoblotting.

TNF ELISA Assay

RAW264.7 cells were maintained in DMEM media supplemented with 10 % heat-inactivated FBS and 1 % antibiotic-antimycotic mix (ThermoFisher Scientific). RAW264.7 cells were seeded into 12 well plates at a density of $1.5x10^5$ cells/well in 1 mL of media. Inhibitors were diluted and added in 1 µL DMSO 15 min prior to the addition of 10 µg/mL MDP or 10 ng/mL E. coli LPS for 24 h. For TNF measurements, 100 µL of undiluted media (MDP) or 5-fold diluted media was analyzed using Duo-Set anti-mouse TNF ELISA kit (R&D Systems). Values of media-only wells were subtracted and %inhibition for each compound concentration relative to the DMSO/MDP (or LPS)-treated controls were calculated. IC50 values were calculated using Prism software (GraphPad).

References

1. Girardin, S. E., Travassos, L. H., Herve, M., Blanot, D., Boneca, I. G., Philpott, D. J., Sansonetti, P. J., and Mengin-Lecreulx, D. (2003) Peptidoglycan molecular requirements allowing detection by Nod1 and Nod2. *The Journal of biological chemistry* **278**, 41702-41708
2. Damgaard, R. B., Nachbur, U., Yabal, M., Wong, W. W., Fiil, B. K., Kastirr, M., Rieser, E., Rickard, J. A., Bankovacki, A., Peschel, C., Ruland, J., Bekker-Jensen, S., Mailand, N., Kaufmann, T., Strasser, A., Walczak, H., Silke, J., Jost, P. J., and Gyrd-Hansen, M. (2012) The ubiquitin ligase XIAP recruits LUBAC for NOD2 signaling in inflammation and innate immunity. *Molecular cell* **46**, 746-758
3. Hugot, J. P., Chamaillard, M., Zouali, H., Lesage, S., Cezard, J. P., Belaiche, J., Almer, S., Tysk, C., O'Morain, C. A., Gassull, M., Binder, V., Finkel, Y., Cortot, A., Modigliani, R., Laurent-Puig, P., Gower-Rousseau, C., Macry, J., Colombel, J. F., Sahbatou, M., and Thomas, G. (2001) Association of NOD2 leucine-rich repeat variants with susceptibility to Crohn's disease. *Nature* **411**, 599-603
4. Ogura, Y., Bonen, D. K., Inohara, N., Nicolae, D. L., Chen, F. F., Ramos, R., Britton, H., Moran, T., Karaliuskas, R., Duerr, R. H., Achkar, J. P., Brant, S. R., Bayless, T. M., Kirschner, B. S., Hanauer, S. B., Nunez, G., and Cho, J. H. (2001) A frameshift mutation in NOD2 associated with susceptibility to Crohn's disease. *Nature* **411**, 603-606
5. Negroni, A., Stronati, L., Pierdomenico, M., Tirindelli, D., Di Nardo, G., Mancini, V., Maiella, G., and Cucchiara, S. (2009) Activation of NOD2-mediated intestinal pathway in a pediatric population with Crohn's disease. *Inflamm Bowel Dis* **15**, 1145-1154
6. Caso, F., Galozzi, P., Costa, L., Sfriso, P., Cantarini, L., and Punzi, L. (2015) Autoinflammatory granulomatous diseases: from Blau syndrome and early-onset sarcoidosis to NOD2-mediated disease and Crohn's disease. *RMD Open* **1**, e000097
7. Jurynec, M. J., Sawitzke, A. D., Beals, T. C., Redd, M. J., Stevens, J., Otterud, B., Leppert, M. H., and Grunwald, D. J. (2018) A hyperactivating proinflammatory RIPK2 allele associated with early-onset osteoarthritis. *Hum Mol Genet*

8. Inaki, K., Menghi, F., Woo, X. Y., Wagner, J. P., Jacques, P. E., Lee, Y. F., Shreckengast, P. T., Soon, W. W., Malhotra, A., Teo, A. S., Hillmer, A. M., Khng, A. J., Ruan, X., Ong, S. H., Bertrand, D., Nagarajan, N., Karuturi, R. K., Miranda, A. H., and Liu, E. T. (2014) Systems consequences of amplicon formation in human breast cancer. *Genome Res* **24**, 1559-1571
9. Canning, P., Ruan, Q., Schwerd, T., Hrdinka, M., Maki, J. L., Saleh, D., Suebsuwong, C., Ray, S., Brennan, P. E., Cuny, G. D., Uhlig, H. H., Gyrd-Hansen, M., Degterev, A., and Bullock, A. N. (2015) Inflammatory Signaling by NOD-RIPK2 Is Inhibited by Clinically Relevant Type II Kinase Inhibitors. *Chem Biol* **22**, 1174-1184
10. Nachbur, U., Stafford, C. A., Bankovacki, A., Zhan, Y., Lindqvist, L. M., Fiil, B. K., Khakham, Y., Ko, H. J., Sandow, J. J., Falk, H., Holien, J. K., Chau, D., Hildebrand, J., Vince, J. E., Sharp, P. P., Webb, A. I., Jackman, K. A., Muhlen, S., Kennedy, C. L., Lowes, K. N., Murphy, J. M., Gyrd-Hansen, M., Parker, M. W., Hartland, E. L., Lew, A. M., Huang, D. C., Lessene, G., and Silke, J. (2015) A RIPK2 inhibitor delays NOD signalling events yet prevents inflammatory cytokine production. *Nature communications* **6**, 6442
11. Tigno-Aranjuez, J. T., Benderitter, P., Rombouts, F., Deroose, F., Bai, X., Mattioli, B., Cominelli, F., Pizarro, T. T., Hoflack, J., and Abbott, D. W. (2014) In vivo inhibition of RIPK2 kinase alleviates inflammatory disease. *The Journal of biological chemistry* **289**, 29651-29664
12. Vasta, J. D., Corona, C. R., Wilkinson, J., Zimprich, C. A., Hartnett, J. R., Ingold, M. R., Zimmerman, K., Machleidt, T., Kirkland, T. A., Huwiler, K. G., Ohana, R. F., Slater, M., Otto, P., Cong, M., Wells, C. I., Berger, B. T., Hanke, T., Glas, C., Ding, K., Drewry, D. H., Huber, K. V. M., Willson, T. M., Knapp, S., Muller, S., Meisenheimer, P. L., Fan, F., Wood, K. V., and Robers, M. B. (2018) Quantitative, Wide-Spectrum Kinase Profiling in Live Cells for Assessing the Effect of Cellular ATP on Target Engagement. *Cell Chem Biol* **25**, 206-214 e211
13. Mohedas, A. H., Wang, Y., Sanvitale, C. E., Canning, P., Choi, S., Xing, X., Bullock, A. N., Cuny, G. D., and Yu, P. B. (2014) Structure-activity relationship of 3,5-diaryl-2-aminopyridine ALK2 inhibitors reveals unaltered binding affinity for fibrodysplasia ossificans progressiva causing mutants. *J Med Chem* **57**, 7900-7915
14. Doench, J. G., Fusi, N., Sullender, M., Hegde, M., Vaimberg, E. W., Donovan, K. F., Smith, I., Tothova, Z., Wilen, C., Orchard, R., Virgin, H. W., Listgarten, J., and Root, D. E. (2016) Optimized sgRNA design to maximize activity and minimize off-target effects of CRISPR-Cas9. *Nat Biotechnol* **34**, 184-191
15. Haile, P. A., Casillas, L. N., Bury, M. J., Mehlmann, J. F., Singhaus, R. Jr., Charnley, A. K., Hughes, T. V., DeMartino, M. P., Wang, G. Z., Romano, J. J., Dong, X., Plotnikov, N. V., Lakdawala, A. S., Convery, M. A., Votta, B. J., Lipshutz, D. B., Desai, B. M., Swift, B., Capriotti, C. A., Berger, S. B., Mahajan ,M. K., Reilly, M. A., Rivera, E. J., Sun, H. H., Nagilla, R., LePage, C., Ouellette, M. T., Totoritis, R. D., Donovan, B. T., Brown, B. S., Chaudhary, K. W., Gough, P. J., Bertin, J., Marquis, R. W. . (2018) Identification of Quinoline-Based RIP2 Kinase Inhibitors with an Improved Therapeutic Index to the hERG Ion Channel. *ACS Med Chem Lett* **9**, 1039-1044
16. Kabsch, W. (2010) Xds. *Acta Crystallogr D Biol Crystallogr* **66**, 125-132
17. Evans, P. R., and Murshudov, G. N. (2013) How good are my data and what is the resolution? *Acta Crystallogr D Biol Crystallogr* **69**, 1204-1214
18. Winn, M. D., Ballard, C. C., Cowtan, K. D., Dodson, E. J., Emsley, P., Evans, P. R., Keegan, R. M., Krissinel, E. B., Leslie, A. G., McCoy, A., McNicholas, S. J., Murshudov, G. N., Pannu, N. S., Potterton, E. A., Powell, H. R., Read, R. J., Vagin, A., and Wilson, K. S. (2011) Overview of the CCP4 suite and current developments. *Acta Crystallogr D Biol Crystallogr* **67**, 235-242
19. McCoy, A. J., Grosse-Kunstleve, R. W., Adams, P. D., Winn, M. D., Storoni, L. C., and Read, R. J. (2007) Phaser crystallographic software. *J Appl Crystallogr* **40**, 658-674
20. Adams, P. D., Afonine, P. V., Bunkoczi, G., Chen, V. B., Davis, I. W., Echols, N., Headd, J. J., Hung, L. W., Kapral, G. J., Grosse-Kunstleve, R. W., McCoy, A. J., Moriarty, N. W., Oeffner, R., Read, R. J., Richardson, D. C., Richardson, J. S., Terwilliger, T. C., and Zwart, P. H. (2010) PHENIX: a comprehensive Python-based system for macromolecular structure solution. *Acta Crystallogr D Biol Crystallogr* **66**, 213-221
21. Murshudov, G. N., Skubak, P., Lebedev, A. A., Pannu, N. S., Steiner, R. A., Nicholls, R. A., Winn, M. D., Long, F., and Vagin, A. A. (2011) REFMAC5 for the refinement of macromolecular crystal structures. *Acta Crystallogr D Biol Crystallogr* **67**, 355-367
22. Emsley, P., Lohkamp, B., Scott, W. G., and Cowtan, K. (2010) Features and development of Coot. *Acta Crystallogr D Biol Crystallogr* **66**, 486-501

23. Painter, J., and Merritt, E. A. (2006) Optimal description of a protein structure in terms of multiple groups undergoing TLS motion. *Acta Crystallogr D Biol Crystallogr* **62**, 439-450
24. Chen, V. B., Arendall, W. B., 3rd, Headd, J. J., Keedy, D. A., Immormino, R. M., Kapral, G. J., Murray, L. W., Richardson, J. S., and Richardson, D. C. (2010) MolProbity: all-atom structure validation for macromolecular crystallography. *Acta Crystallogr D Biol Crystallogr* **66**, 12-21
25. Fiil, B. K., Damgaard, R. B., Wagner, S. A., Keusekotten, K., Fritsch, M., Bekker-Jensen, S., Mailand, N., Choudhary, C., Komander, D., and Gyrd-Hansen, M. (2013) OTULIN restricts Met1-linked ubiquitination to control innate immune signaling. *Molecular cell* **50**, 818-830